Inductive sensor for lightning current measurement, fitted in aircraft windows, part II: Measurements on an A320 aircraft

Inductive Sensor for Lightning Current Measurement, Fitted in Aircraft Windows—Part II: Measurements on an A320 Aircraft

Alexander P. J. van Deursen, *Senior Member, IEEE*

***Abstract*—A novel sensor for the detection of the lightning current through the fuselage of an aircraft has been tested on an A320 aircraft. An accurate method-of-moment model of the window edge provided reliable calibration of the sensor for external fields. The data have been analyzed and the good performance of the sensor in sensitivity and bandwidth is demonstrated.**

***Index Terms*—Aircraft, inductive sensor, lightning, viewport, window.**

I. Introduction

AIRCRAFTS receive a lightning strike once a year on the average. Maintenance after strike would benefit from knowledge of lightning entry and exit points. The In Flight Lightning Damage Assessment System (ILDAS) is designed to retrieve the lightning attachment points [1]. To this end, a number of sensors distributed over the aircraft continuously monitor the local magnetic field. A lightning strike triggers the system to store data over a time span of approximately 1 s. A prototype of the ILDAS system has been tested on an Airbus A320 in Toulouse (F) in the summer of 2009. Twelve magnetic field sensors were used.

Several types of sensors have been developed for ILDAS [2]. A particular sensor was proposed that can be fitted in a window, which is sensitive to the lightning-induced magnetic field along the fuselage. The accompanying paper [3] analyzes the sensitivity of the window sensor for various positions with respect to the assumed circular window opening . There, it became clear that the sensitivity depends on detailed shape of the window metallic parts. In this paper, a numerical method-of-moments (MoM) model provides the sensitivity of the sensor placed in the bottom of a rectangular TEM cell. Comparison of the MoM results for a circular opening with the analytical expressions derived in [3] shows agreement to better than 0.2%. The accuracy of the model sensor in an actual window depends on how well the window mounting is described. It is estimated at 3%.

This paper presents the measurement setup in Section II. Section III compares the current and magnetic field waveform to show the correct operation of the window sensor. The MoM model is detailed in Section IV. A comparison of the magnetic field measured by the window sensors and other sensors is given in Section V, along with the results obtained by a conformal mapping model for the aircraft fuselage. The conclusion is that the sensor fulfils the ILDAS requirements for the recognition of the lightning current pattern on an aircraft.

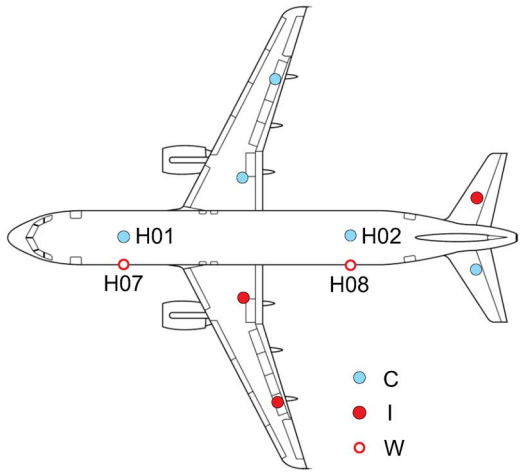

Fig. 1. A320 aircraft with 12 sensor positions indicated. C: Cobham inductive sensors, H01 is on top, H02 at the bottom of the aircraft; I: Ildas LF and HF sensors; W: window sensors H07 and H08.

II. Setup

An A320 aircraft stood above a metal netting on the floor of a hangar. The netting had the shape of a cross under fuselage and wings, and acted as ground plane (GP) and return for the current. Polyethylene sheets insulated the GP with respect to the floor. The discharge of a high-voltage capacitor provided the current. The current waveshape approximated the stroke A-component mentioned in [4]. The amplitude was reduced to about 3 kA because the purpose of the test was to demonstrate the correct operation of the ILDAS system and not to establish the aircraft safety. A Pearson probe recorded the current. The aircraft was instrumented with a mixture of ILDAS and Cobham sensors (Fig. 1), and the magnetic field data were recorded by the ILDAS system and by digital scopes.

Eighteen scenarios were tested, with different current entrance and exit points; the successful outcome of the current pattern recognition has been presented in [1]. In this paper, two measurements with the window sensors in the main current

Manuscript received January 10, 2010; revised May 10, 2010; accepted June 16, 2010. Date of publication September 20, 2010; date of current version November 10, 2010. The associate editor coordinating the review of this manuscript and approving it for publication was Dr. Patrick Ruther.

The author is with the Department of Electrical Engineering, Eindhoven University of Technology, 5600 MB Eindhoven, The Netherlands (e-mail: a.p.j.v.deursen@tue.nl).

Color versions of one or more of the figures in this paper are available online at http://ieeexplore.ieee.org.

Digital Object Identifier 10.1109/JSEN.2010.2055559

Fig. 2. Photograph of a window sensor. Two twisted wires form the central bar. The boxes provide connections and termination of the coaxial cables that act as outer perimeter of the figure-eight. The cables are mostly laid in a region of low magnetic flux, between fuselage and the top rim of the window pane mounting flange.

path are analyzed: current injected at the nose and retrieved at the vertical tail fin as in records 10 and 11 of the series taken on June 9, 2009. A window sensor is shown in Fig. 2.

III. Waveform

The inductive sensors, coils, and window, deliver a signal proportional to the time-derivative of the magnetic field. The signals of the Cobham inductive sensors are integrated numerically in the scopes. A combination of passive and active integrators restored the waveform of the inductive ILDAS sensors. The passive integrators were the first stage and filtered frequencies higher than the band of interest [5]. Active integrators extended the frequency range down to 100 Hz. The signal acquisition chain contained three high-pass filters, two at 100 Hz in the integrator and one at 85 Hz before the analog-to-digital converter (ADC). Special shielded coils and integrators with a bandwidth down to 0.16 Hz could record the quasi-continuous part of the lightning current wave form [6], but these were not implemented in combination with the window sensors. Because the frequency band of interest for the A-component is far above the three crossover frequencies, the response of the window sensor is only slightly affected by the high-pass filters, and a simple procedure redresses the signal. Three time-domain filters, each with a frequency-domain representation $1 + 1/j\omega\tau_i$, correct the recorded window sensor data. Fig. 3 shows the original response for window sensor H08, the corrected response, and the current scaled to the same amplitude and shifted in time for optimal coincidence. The current and corrected responses coincide to within the noise of the data, even after smoothing has been applied to reduce digital noise. At the end of the record, the difference amounts to 1% of the maximum; this can be readily attributed to the limited resolution of the input before correction. The data for sensor H07 give similar results, but are not shown. At frequencies of interest here, the metal parts around the window sensor can be considered to be impenetrable for magnetic fields. This allows the analysis described in Section IV.

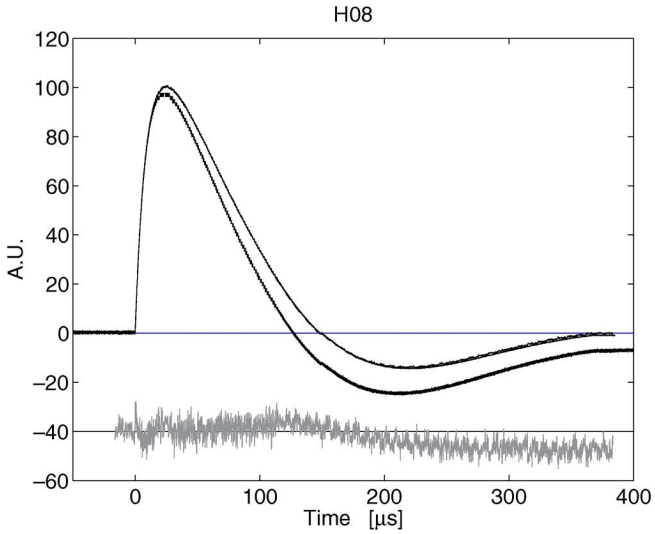

Fig. 3. Output of the integrator for window sensor H08 in arbitrary units, before (lower curve, heavy due to digital noise) and after (upper thin curve) correction for the time constants, in comparison with the current. Corrected output and current are barely distinguishable on this scale. The difference between these is shown, multiplied by a factor of 10 and shifted over −40.

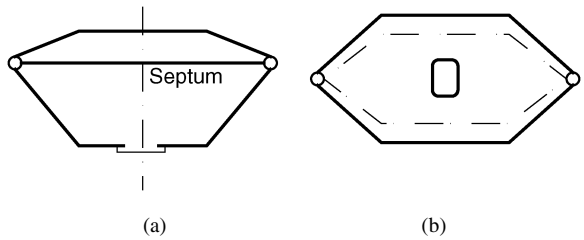

Fig. 4. (a) Midbody cross section of TEM cell, with path of the sensor lead indicated by the thin line at the bottom. (b) Bottom view of the TEM cell with window opening. The septum is indicated by the dashed lines. The circles at the septum ends represent the current sources.

IV. Sensitivity

The interpretation of the window sensor data requires two steps. First, the magnetic field pattern outside the aircraft placed above the GP needs to be known. The nearby return concentrates the current distribution at the bottom the aircraft fuselage (ACF). The concentration depends on the width of the GP. EADS modeled the aircraft by a finite-difference time-domain (FDTD) method, which included the aircraft metallic and nonconducting parts. The FDTD mesh could be rather course compared with the window size, because the magnetic field H_0 at the window position was required, without the window opening. The FDTD input data are EADS proprietary information and this calculation is not discussed here further. A simpler method relies on conformal mapping (CM); details are given in the Appendix. In this method, the ACF is represented by a well-conducting tube above a conducting GP of finite width. The diameter of the ACF is 3.95 m, the GP under the fuselage was 13.2 m wide, and the distance between the ACF bottom and GP was 1.70 m.

Second, the penetration of the magnetic field through the window opening and its mounting needs to be calculated. Point of special attention have been discussed in the accompanying

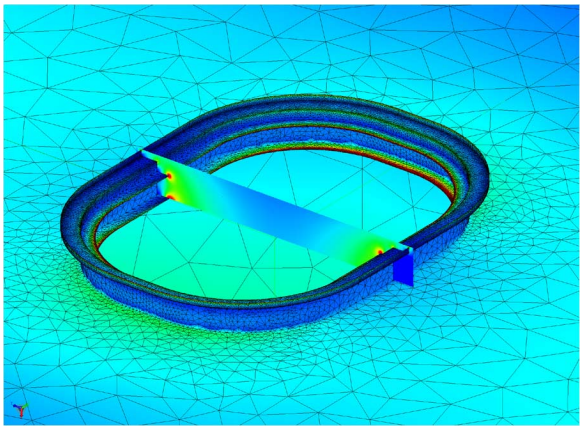

Fig. 5. Meshing, intensity of the electric field, and current density near the window, shown upside down. The window mounting cross section is case c) in Fig. 6.

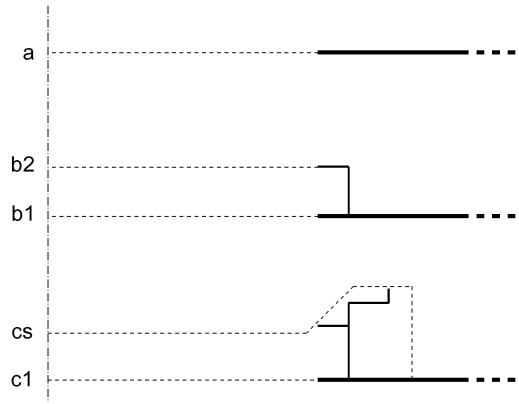

Fig. 6. Three mountings of the window sensor, shown half but with correctly scaled shape. The heavy horizontal lines represent the fuselage extending to the right, thin lines the mounting. Inside is up, outside down. The vertical dashed–dotted line is the center line of the window. Thin dashes indicate the path of integration to obtain the induced voltage. The upper thin dashes in case c are a good approximation of the actual wire path shown in Fig. 2.

paper [3]. The sensor is thought to be mounted at the outside of the bottom of an existing TEM cell [7] which replaced the aircraft. The TEM cell limits the calculation effort. It is a closed structure except for the window opening, and it is excited internally. This guarantees that the effects of the field penetration through the window model prevail. The rectangular measuring section of the TEM cell is 0.91 m long in the direction of current flow, 1.40 m deep, and 0.90 m high. The current carrying septum is asymmetrically placed at the height of 0.72 m, and it is designed to give the TEM cell a wave impedance of 50 Ω. The TEM cell has been modeled by the Feko MoM.[1] Two voltage sources at 2 MHz excite the TEM cell at both ends of the septum. The choice of frequency depends on two factors: wave length effect should not interfere in the quasi-static regime, and the ratio of scalar-to-vector potential contributions must remain manageable with double precision arithmetics. The phases of the voltage sources are chosen opposite in order to enhance the induced electric field over the static field. The variation of H_0 in the x-direction is negligible within the window area. The presence of the side walls causes a parabolic variation of the H_0 field in the y-direction parallel to the long axis of the window. At the window edge, the field is 6% smaller than at the center. Increasing the size of the TEM cell by a factor of 1.5 decreases this variation to 2%, a factor of 2 even down to 0.7%. The 2% variation is acceptable in view of the measurement accuracy. The corresponding scale factor of 1.5 also keeps out-of-core computation time manageable, within 22 h on a 3-GHz, quad core PC with 8-Gbyte memory. The magnetic field H_0 at the bottom is then 199 A/m per kA of current, in absence of the window.

A circular window of radius $r_0 = 0.165$ m is calculated first and acts as "calibration" because an analytical expression for the sensitivity is available; see [3]. The actual window has the shape of a rounded rectangle of 0.33 × 0.23 m (Fig. 5). The long axis stands perpendicular to the current flow, as in the fuselage. Its length is twice the circle radius r_0. Several approximations of the conducting parts of the window mounting have been studied and are given here:

[1]Online. Available: http://www.feko.info/.

TABLE I
VALUES FOR EFFECTIVE FLUX CAPTURING AREA A OF THE SENSOR, IN UNITS OF cm^2. THE FIELD INTEGRATION PATHS ARE INDICATED IN Fig. 6

path:	1	2	sensor
r = 16.5 cm	271.9	–	–
Sens. a	240.2	–	–
Sens. b	217.0	192.4	–
Sens. c	202.7	183.3	184.2

a) window-sized opening in a flat panel;
b) with additional U-shaped mounting flange;
c) with mounting flange approximating the actual shape.

The cases a)–c) refer to the shape of the shapes shown in Fig. 6. The sides of the triangular MoM elements are 5 up to 7 cm on the body of the TEM cell and reduce to 1 mm near the sharp edges of the window opening. The number of elements varies between 20 and 60× 10^3. Meshing, current density, and intensity of the electric field for case c) are shown in Fig. 5. The induced voltages are obtained by integrating the electric field in the middle plane over the thin dashed lines indicated in Fig. 6. Integration occurs by the trapezium rule up to 5 mm from sharp edges. In order to deal with the diverging nature of the fields near those edges, field values between 1–5 mm from an edge are fitted to the expected $1/\sqrt{1-(r/r_0)^2}$ behavior for the circle and integrated analytically. A similar fit is used for the windows. The voltages can be converted into sensitivity of the sensor, expressed as effective flux capturing area A

$$V = j\omega\mu_0 A H_0 \tag{1}$$

where μ_0 the permeability of free space. Table I summarizes the values for A. The effective area of the circle agrees within 0.2% with the analytical expression $r_0^2 = 272.3$ cm^2. Because of the agreement, there was no need felt to sacrifice the TEM cell and actually make the opening in the bottom. The value of A for case a) is the maximum attainable for the window. As case b1) shows, the presence of a second rim deeper inside reduces the sensitivity appreciably. The path c2) is similar to b2), but it is not shown in Fig. 6 for the sake of clarity. The actual sensor has about 77% of the sensitivity of case a without

TABLE II
MAGNETIC FIELD AT FOUR SENSORS FOR AN INJECTION CURRENT $I_{\mathrm{inj}} = 3.11$ kA

	H_{01}	H_{02}	H_{07}	H_{08}
Rec. 10	114	466	148	158
Rec. 11	114	464	147	158
CM	119	503	167	167
FDTD	–	–	141	–

flanges. Based on the variation between cases b2) and c2), the accuracy is estimated better than 3%.

V. MAGNETIC FIELD MEASUREMENTS ON THE A320

The measurements were taken with an injected current of 3.11-kA maximum value. Table II gives the corresponding magnetic fields maxima. Those for the window sensors are based on the effective area of Table I and have been corrected for the signal transfer, as discussed in Section III. Both recordings 10 and 11 show consistent results. The table also includes the magnetic fields determined by the CM method. The H_{01} field is within 2%, and the H_{02} is within 6% of the CM value. The ratio of H_{02} and H_{01} is of interest here. It depends sensitively on several factors: the radius of aircraft, the distance between ground plane and fuselage bottom, and the actual width of the ground plane. The latter is prone to inaccuracy, since the assumed ground plane may be effectively widened by currents induced in the reinforcement of the concrete floor. The actual ratio of 4.08 compared reasonably well with the calculated value by CM: 4.23. An infinitely wide GP would result in a ratio of 3.32, a thin wire in a ratio of 11.

The position of the window center is 2.56 m above the ACF bottom. The window sensor shown in Fig. 2 has a figure-eight configuration, as discussed in [3]. The effective areas of Table I should then be multiplied by a factor of 2. The measured H_{07} field is 12% less than calculated by CM, the H_{08} field 5%. This agreement is acceptable, in view of the limitations of the CM method which fully omits the wings and GP thereunder. The measured value for the H_{07} sensor [8] deviates by about 5% from the FDTD value, calculated for a fuselage diameter of 4.1 m. If the diameter would be scaled to the actual 3.95 m through CM, the field would become 144 A/m, and the agreement would be even better.

VI. CONCLUSION

The window sensor accurately determines the wave shape of the magnetic field outside the aircraft. Details of the window edge and mounting influence the sensitivity, and these have been considered carefully in a MoM approach with fine local mesh. With the aircraft on the ground, the accuracy of the measurements also depends on the current distribution in nearby conductors such as the floor under the ground plane. Such items are difficult to model. Still, the recorded magnetic field amplitudes are consistent with the other sensors used in the tests on the A320. The window sensor measurements agree within the ILDAS requirement of 10% well with the FDTD value available and reasonably well with a simple conformal mapping model for the aircraft. This accuracy shows that the window sensor is well suited for the current pattern recognition on aircraft during lightning strike, which is the final goal of the ILDAS system. The main benefit of this sensor is the simple mounting, which does not require components extending outside the fuselage.

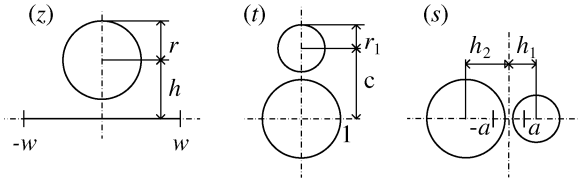

Fig. 7. Two transformations to change the ACF over a GP of finite width into a line dipole.

APPENDIX

The magnetic field around an ACF above a GP of finite width can be obtained by conformal mapping in a 2-D approximation. The GP is mapped onto a circle, and the ACF and GP circle are considered as a magnetic dipole consisting of two lines. The required transformations are shown in Fig. 7. In the complex z-plane, the ACF has a radius r with the center at ih. It is placed above a GP that extends over the real axis, centered at the origin between $(-w, w)$. Both the ACF and GP are assumed impenetrable for the magnetic field, which allows conformal mapping to calculate the magnetic field. The Joukowski transform (2) [9, pp. 58–60] maps the outside of the GP onto a circle of radius 1 centered at the origin in the t-plane

$$t(z) = \frac{z}{w} + \sqrt{\frac{z}{w} + 1} \cdot \sqrt{\frac{z}{w} - 1} \tag{2}$$

$$s(t) = -it + h_2. \tag{3}$$

The ACF remains a circle, with now modified radius r_1 and center position ic. The transformation s [(3)] rotates and shifts both circles. The new center positions $h_{1,2}$ and r_1 are obtained by the requirement that both circles are equiflux lines in a bipolar system with the focus points on the real axis at $\pm a$

$$h_1 = \frac{c^2 + r_1^2 - r_2^2}{2c} \tag{4}$$

$$h_2 = \frac{c^2 - r_1^2 + r_2^2}{2c} \tag{5}$$

$$a = \sqrt{h_1^2 - r_1^2} \tag{6}$$

where $c = h_1 + h_2$. The complex potential $\Omega(s) = X(s) + i\Psi(s)$ describes the magnetic field

$$\mathbf{H(s)} = (\partial X/\partial u, \partial X/\partial v) \tag{7}$$

where $s = u + iv$. For the line dipole with current I through the conductor at a, returning through a conductor at $-a$, one has

$$\Omega(s) = \frac{-iI}{2\pi} \left[\log(s - a) - \log(s + a)\right] \tag{8}$$

where the principal value of the logarithm is understood. The magnitude of the magnetic field at any place in the z-plane is given by $H = |\mathrm{d}\Omega/\mathrm{d}z|$ [10, p. 58].

ACKNOWLEDGMENT

The author would like to thank A. de Boer and M. Bardet, NLR, The Netherlands, J. Hardwick, Cobham Technical Services, U.K., and I. Revel, EADS Innovation Works, Finland, for sharing the procedures, measurement and model data, and photographs of the June 2009 measurement campaign.

REFERENCES

[1] R. Zwemmer, M. Bardet, A. de Boer, J. Hardwick, K. Hawkins, D. Morgan, M. Latorre, N. Marchand, J. Ramos, I. Revel, and W. Tauber, "In-flight lightning damage assessment system (ILDAS); results of the concept prototype tests," in *Proc. ICOLSE*, Pittsfield, US, 2009, Session 9, paper AAA-1.

[2] V. Stelmashuk, A. van Deursen, and R. Zwemmer, "Sensor development for the ILDAS project," in *Proc. EMC Europe Workshop*, Paris, France, Jun. 2007.

[3] A. van Deursen and V. Stelmashuk, "Inductive sensor for lightning current measurement, fitted in aircraft windows—Part I: Analysis for a circular window," *IEEE J. Sensors*, this issue.

[4] "ED-84 Aircraft Lightning Environment and Related Test Waveforms Standards," EUROCAE, Paris, France, EUROCAE WG-31 and SAE committee AE4L, 1997.

[5] V. Stelmashuk, A. van Deursen, and M. Webster, "Sensors for in-flight lightning detection on aircraft," in *Proc. EMC Europe*, Hamburg, Germany, Sep. 2008, pp. 269–274.

[6] A. van Deursen and V. Stelmashuk, "Sensors for in-flight lightning detection on passengers aircrafts," in *Proc. ESA Workshop Aerospace EMC*, Florence, Italy, Mar. 30–1 Apr. 2009, Session 6, paper 2.

[7] M. L. Crawford, "Generation of standard EM fields using TEM transmission cells," *IEEE Trans. Electromagn. Compat.*, vol. EMC-16, no. 4, pp. 189–195, Nov. 1974.

[8] M. Latorré and I. Revel, "ILDAS: Reconstruction d'un courant foudre par méthode inverse utilisant des simulation FDTD," in *Proc. CEM*, Limoges, France, Apr. 7–9, 2010, pp. E2–E4.

[9] H. Kober, *Dictionary of Conformal Representation*. New York: Dover, 1957.

[10] H. Kaden, *Wirbelströme und Schirmung in der Nachrichtentechnik*. Berlin, Germany: Springer, 1959.

Alexander P. J. van Deursen (A'97–SM'97) received the Ph.D. degree in physics from Radboud University, Nijmegen, The Netherlands, in 1976.

He was a Postdoctoral Researcher with the Max Planck Institut fur Festkörperforschung, Hochfeld Magnetlabor, Grenoble, France. He returned to Nijmegen, where he worked on solid-state physics on electronic structures of metals, alloys, and semiconductors by high magnetic field techniques. In 1986, he joined the Eindhoven University of Technology, Eindhoven, The Netherlands, and shifted his attention to electromagnetic compatibility (EMC). He has also been engaged in several International Electrotechnical Commissions (IEC) working groups. He has been the Chairman and member of different committees in international conferences. He is a member of the International Steering Committee of EMC Europe and is Vice-Chairman of URSI Commission E.